Strain induced ferromagnetism in Sb co-doped ZnMnO samples

2009 J. Phys.: Condens. Matter 21 296001

(http://iopscience.iop.org/0953-8984/21/29/296001)

J. Phys.: Condens. Matter **21** (2009) 296001 (6pp) doi:10.1088/0953-8984/21/29/296001

Strain induced ferromagnetism in Sb co-doped ZnMnO samples

V K Sharma and G D Varma

Department of Physics, Indian Institute of Technology Roorkee, Roorkee-247 667, India

E-mail: gdvarfph@iitr.ernet.in

Received 10 February 2009, in final form 4 April 2009
Published 29 June 2009
Online at stacks.iop.org/JPhysCM/21/296001

Abstract

We report on the effect of Sb co-doping on the structural and magnetic properties of bulk ZnMnO samples. Samples with nominal compositions $Zn_{0.98-y}Mn_{0.02}Sb_yO$ ($y = 0$, 0.01 and 0.03) were synthesized using a solid state reaction route at 800 °C. X-ray diffraction (XRD) results reveal wurtzite structure of pure ZnO without any impurity phases for compositions $y = 0.0$ and 0.01. On the other hand, a weak diffraction peak corresponding to the impurity phase $Zn/MnSb_2O_6$ was detected in the XRD pattern of composition $y = 0.03$. Energy dispersive x-ray (EDAX) results confirm the presence of all elements in the samples in the stoichiometric ratio. The M–H curve of the pure ZnMnO sample shows paramagnetic behavior, whereas M–H curves of Sb co-doped samples show room temperature ferromagnetism (RTFM) with saturated loops. Saturation magnetization (M_S) and coercive field (H_C) both increase with the increase in Sb doping percentage. Inverse susceptibility ($1/\chi$) versus temperature (T) curves suggests dominant antiferromagnetic interactions in the samples which decrease with the co-doping of Sb. Based on the experimental results we conclude that the observed RTFM in Sb co-doped ZnMnO is due to defects induced by strain.

(Some figures in this article are in colour only in the electronic version)

1. Introduction

Diluted magnetic semiconductors (DMSs) have attracted wide interest and there has been a major effort to produce DMSs with a Curie temperature (T_C) above room temperature (RT). DMSs are usually produced by doping semiconductors with transition metals (TMs). ZnO and GaN were theoretically predicted to be ideal candidates for RT DMSs [1]. Even though ferromagnetism (FM) has been observed in Mn doped ZnO, experimental studies have produced inconsistent results and the mechanism of FM in Mn doped ZnO remains unclear. Magnetic results reported for these DMSs varies from paramagnetic [2, 3], ferromagnetic [4, 5], antiferromagnetic [6–8] to spin glass behavior [9]. FM behavior was observed in both insulating as well as semiconducting samples, and two distinct mechanisms—magnetic polarons and carrier mediated exchange—were proposed for the observed FM. The most widely accepted picture for the FM in DMSs is carrier mediated exchange. Therefore, some work has been done with additional dopants [10, 11] to enhance or induce FM.

ZnO has electron (n-type) conductivity with appropriate dopants such as Al, Ga etc. Heavy electron doping of up to 10^{21} cm^{-3} can be realized in ZnO by using a proper doping technique. There are a lot of reports on Al co-doped Zn(Mn/Co)O samples [12–17]. Liu *et al* [12] found room temperature ferromagnetism (RTFM) in Al co-doped ZnCoO through the increase in carrier concentration by doping a few per cent of Al. Fukumura *et al* [13, 14] obtained highly conductive n-type $Zn_{1-x}Mn_xO$ films after doping with Al. Zhang *et al* [15], on the basis of first-principles calculations, showed that additional electrons induced by Al doping can stabilize the ferromagnetic state in Co doped ZnO. The additional electrons act as carrier media to stabilize the FM state with composite mechanisms consisting of both Ruderman–Kittel–Kasuya–Yosida and double-exchange interactions. Careful analysis of the reports revealed that besides the carriers, structural defects are also important for the observed FM [16]. Xu *et al* [17] found carrier induced RTFM in n-type ZnMnAlO and ZnCoAlO thin films. The reported values of the magnetic moments by this group are close to the ideal value and also have a substantial ($\sim 10^{21}$ cm^{-3}) carrier density. Carrier mediated FM is also reported by using Cu as

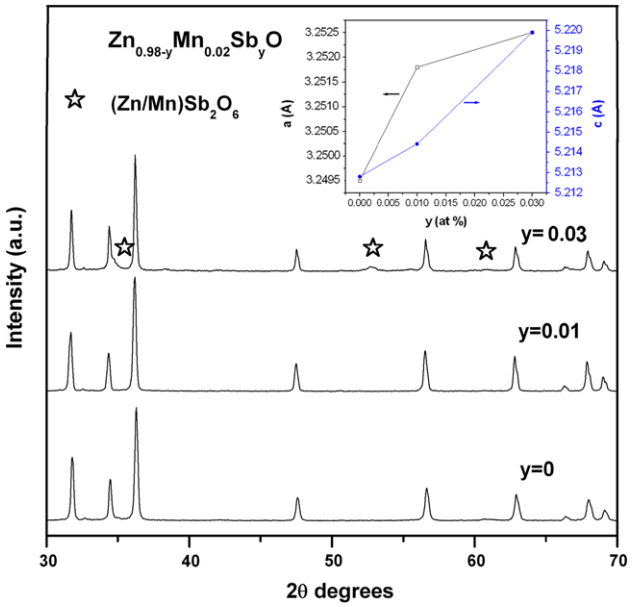

Figure 1. X-ray diffraction pattern of $Zn_{0.98-y}Mn_{0.02}Sb_yO$ (the inset shows the variation of lattice parameters with Sb concentration).

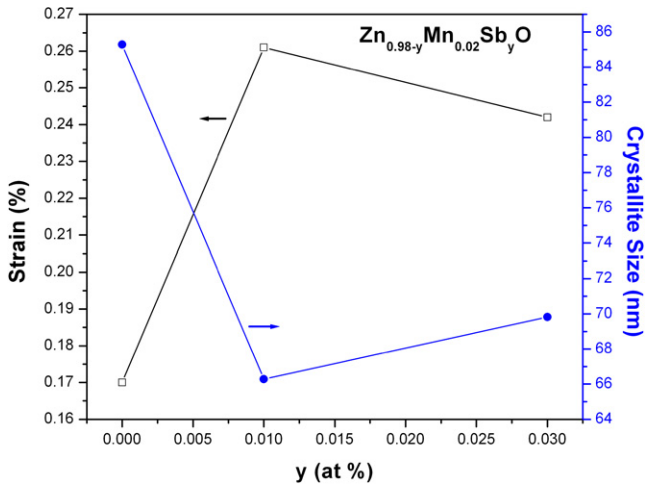

Figure 2. Variation of strain and crystallite size with Sb co-doping concentration.

an additional dopant in ZnCoO [18, 19]. Recently, RTFM has been reported in Sb co-doped ZnMnO thin films synthesized by radio-frequency magnetron sputtering [20]. Sb doped p-type ZnO films are reported by a few groups [21, 22] but Sb co-doped ZnMnO still remains mostly unexplored. To the best our knowledge there is only one paper on Sb co-doped ZnMnO films [20] and no paper on its bulk counterpart. In this paper we have investigated the effect of Sb co-doping on the structural and magnetic properties of bulk ZnMnO samples.

2. Experiments

Bulk samples with nominal compositions $Zn_{0.98-y}Mn_{0.02}Sb_yO$ ($y = 0.0$, 0.01 and 0.03) were synthesized by the standard solid state reaction route. In this route, appropriate amounts of ZnO, MnO_2 and Sb_2O_3 were mixed according to the required composition and ground in an agate mortar. The resulting powder was heated at 400 °C for 10 h in air followed by furnace cooling down to RT. After this, the resulting material was reground and pelletized. Finally, the pellets were sintered at 800 °C in air for 12 h followed by furnace cooling. The crystal structure of the samples was studied using an x-ray diffractometer (XRD) employing Cu Kα (1.54 Å) radiation. The temperature dependence of the magnetization (M–T) and magnetic hysteresis (M–H) loops were measured using a vibrating sample magnetometer (VSM) and superconducting quantum interference devices (SQUIDs). Microstructural and chemical analysis of the samples was carried out using a field emission scanning electron microscope (FESEM) equipped with an energy dispersive x-ray (EDAX) detector.

3. Results and discussion

Figure 1 shows the XRD patterns of $Zn_{0.98-y}Mn_{0.02}Sb_yO$ samples. In the XRD patterns of Sb co-doped samples of compositions $y = 0.0$ and 0.01 all the diffraction peaks correspond to the wurtzite structure of pure ZnO. However, there are a few weak peaks corresponding to secondary phase $(Zn/Mn)Sb_2O_6$ in the Sb co-doped sample of composition $y = 0.03$. Further, it has been observed that the lattice parameters increase with the Sb doping concentration (see inset of figure 1). This confirms that doped Sb (ionic radius of $Sb^{3+} \sim 92$ pm) substitute at Zn sites (ionic radius of $Zn^{2+} \sim 74$ pm).

We have calculated the strain from a Williamson–Hall plot [23] using XRD data. The Williamson–Hall equation is expressed as follows:

$$B\cos\theta = K\lambda/D + 2(\varepsilon)\sin\theta \qquad (1)$$

where B is the full width at half maximum (FWHM) of the XRD peaks, K is the Scherer constant (∼0.89), D is the crystallite size, λ is the x-ray wavelength (∼1.54 Å), ε is the lattice strain and θ is the Bragg angle. In this method, $B\cos\theta$ is plotted against $2\sin\theta$. The intercept of the linear plot gives the particle size ($K\lambda/D$) and its slope gives the strain (ε). In our case, we found that crystallite size decreases with increase in the Sb concentration whereas strain increases (see figure 2).

The magnetization versus magnetic field (M–H) curves recorded at 300 K (RT) for all the samples of composition $Zn_{0.98-y}Mn_{0.02}Sb_yO$ ($y = 0.0$, 0.01 and 0.03) are shown in figure 3. For the M–H measurements the samples were taken in powder form and the diamagnetic contribution from the sample holder has been subtracted. The M–H curve of the $Zn_{0.98}Mn_{0.02}O$ sample shows linear variation of magnetization with magnetic field, suggesting paramagnetic behavior of the sample. On the other hand, the M–H curves of the Sb co-doped samples show the presence of hysteresis loops. The variation of M_S and H_C with Sb doping percentage is shown in the inset of figure 3. It has been observed that both M_S and H_C increase with increase in the Sb doping percentage. The increase of H_C with decrease in crystallite size can be explained by the increase in domain wall pinning due to the greater number of lattice defects in small grain size

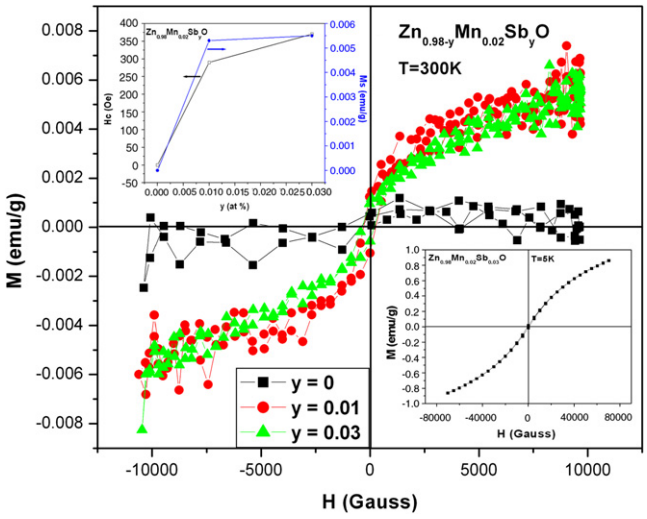

Figure 3. M–H curves of Sb co-doped ZnMnO. The lower inset shows the M–H curve at 5 K and the upper inset shows the variation of coercive field (H_C) and saturation magnetization (M_S) with Sb concentration.

samples [24]. Thus we found that FM increases with increase in Sb doping percentage. The M–H curve for the $y = 0.03$ sample recorded at 5 K is shown in the inset of figure 3. Normally, for magnetic materials at low temperatures, a better signal is expected. But magnetization measurements at 5 K showed a signal with a small kink around the origin, indicating small but definite ferromagnetic ordering along with significant paramagnetic and superparamagnetic components. Thus it can be concluded that only some portion of the substituted Mn^{2+} ions are in a ferromagnetic state and the rest are in a paramagnetic/antiferromagnetic state which may be the reason for the small value ∼0.0055 emu g^{-1} (∼$0.082 \times 10^{-3} \mu_B$/Mn) of M_S rather than the theoretical value (∼5 μ_B/Mn). The impurity phase $MnSb_2O_6$ observed in the XRD is reported to be a paramagnet at RT [25]. Therefore its contribution to the observed RTFM is ruled out.

We have also recorded the temperature dependent magnetization (M–T curves) of $Zn_{0.98-y}Mn_{0.02}Sb_yO$ samples using a SQUID magnetometer in the temperature range 5–300 K. The zero-field-cooled (ZFC) and field-cooled (FC) M–T curves, measured by applying a magnetic field of 500 Oe, for the samples $y = 0$ and 0.03 are shown in figure 4. By comparing the FC curves of $y = 0$ and 0.03 samples at low temperatures we see that magnetic moment of the $y = 0$ sample is greater than that of the $y = 0.03$ sample. Since the low temperature regime shows paramagnetic behavior, the paramagnetic fraction in the $y = 0.03$ sample is small compared to the $y = 0$ sample. This is because of the introduction of FM in the $y = 0.03$ sample. By carefully analyzing the M–T behavior of the $Zn_{0.98}Mn_{0.02}O$ sample in the low temperature regime (see figure 4(a)), we see a clear deviation in the ZFC–FC curve at ∼13 K. This deviation is a feature of spin glass behavior [9, 26] and is probably due to the simultaneous presence of competing (paramagnetic/antiferromagnetic) interactions and disorder. This type of behavior is not present in Sb co-doped samples,

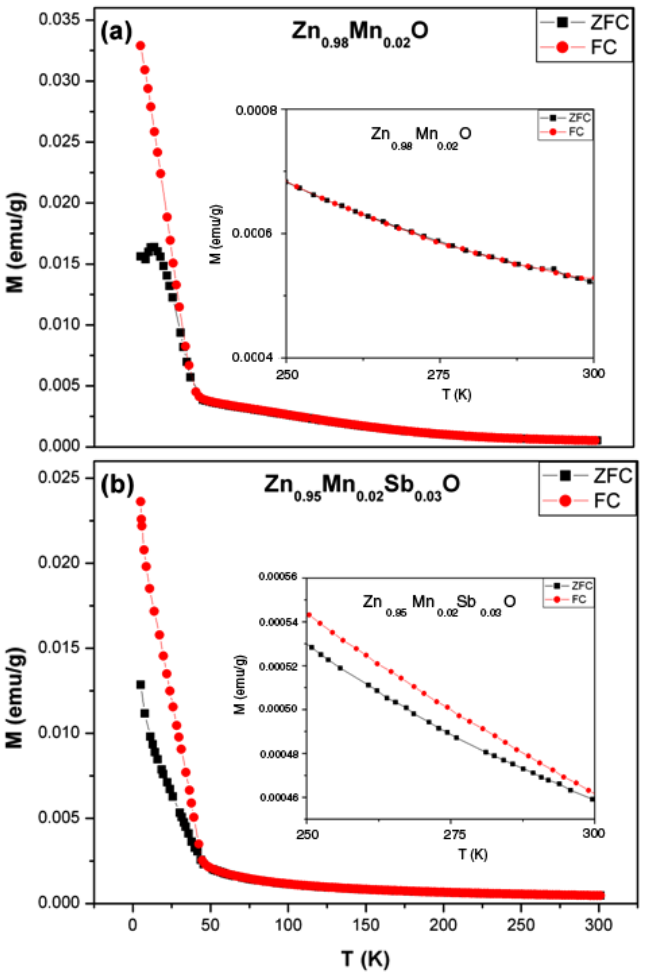

Figure 4. ZFC–FC M–T curves for $Zn_{0.98}Mn_{0.02}Sb_yO$: (a) $y = 0$ and (b) $y = 0.03$. The inset shows expansion of ZFC–FC curves in the region of 250–300 K.

which further substantiates that introduction of Sb helps in stabilizing FM in the ZnMnO samples. The difference in the ZFC and FC curves persists up to RT (see inset of figure 4) for the $y = 0.03$ sample, which is also supported by the ferromagnetic M–H curve recorded at 300 K. For $y = 0$, the figure shows overlapping of the ZFC and FC curves, implying paramagnetic behavior of the sample at RT, which is also supported by the M–H curve recorded at 300 K. The difference between ZFC and FC gives the net magnetization value (ΔM = FC − ZFC) corresponding to the ferromagnetic contribution in the sample by eliminating the para- and diamagnetic contributions [27]. The net magnetization ΔM is, however, very small at 300 K. This suggests weak FM in the sample at RT.

The plots of inverse susceptibility ($1/\chi$) as a function of temperature (T) of the $y = 0.0$ and 0.03 samples are shown in figure 5. The linear regime of each $1/\chi$ versus T curve is fitted with the Curie–Weiss linear relation as

$$\chi = C(x)/(T - \theta(x)) \tag{2}$$

where $\theta(x)$ is the Curie–Weiss temperature and $C(x)$ is the Curie constant. We have estimated $\theta(x)$ from the linear fit in

Table 1. Various parameters obtained from the susceptibility data.

Sample	Θ_0 (K)	C_M (emu K g^{-1} Oe^{-1})	μ_{eff} (μ_B)	J (total quantum number)	$2J_{\text{ex}}/k_B$
$Zn_{0.98}Mn_{0.02}O$	−140	0.0212	0.423	1.04	−16.49
$Zn_{0.95}Mn_{0.02}Sb_{0.03}O$	−70	0.0244	0.488	1.05	−8.13

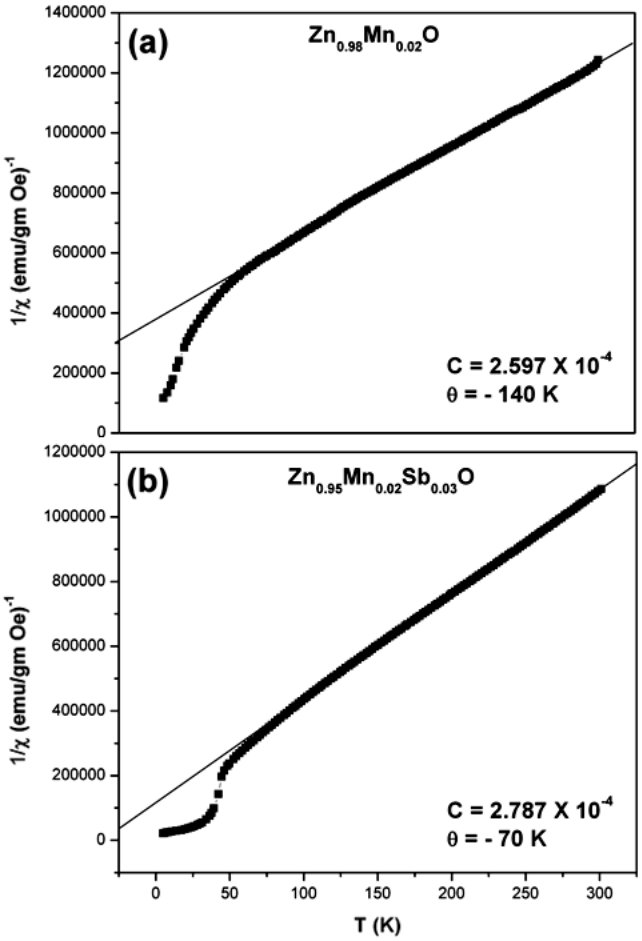

Figure 5. Inverse susceptibility ($1/\chi$) versus temperature (T) curves for $Zn_{0.98}Mn_{0.02}Sb_yO$: (a) $y = 0$ and (b) $y = 0.03$.

the experimental curves as shown in figure 5. The values of $\theta(x)$ are found to be −140 K and −70 K for $Zn_{0.98}Mn_{0.02}O$ and $Zn_{0.95}Mn_{0.02}Sb_{0.03}O$ samples, respectively. This analysis confirms that the magnetic interaction in these systems is antiferromagnetic (AFM) in nature.

From the Curie–Weiss fit of the $1/\chi$ versus T curves, the μ_{eff} (effective Bohr magneton number) per gram can be calculated from the slope $C(x)^{-1}$. $C(x)$ is related to the μ_{eff} through the relation

$$\mu_{\text{eff}} = [3k_B C(x)/N_A]^{1/2} \tag{3}$$

where k_B is the Boltzmann constant and N_A is the Avogadro number. Also

$$\mu_{\text{eff}} = g[J(J+1)]^{1/2}\mu_B \tag{4}$$

where μ_B is the Bohr magneton number and g is the Landé g factor. From equations (3) and (4), considering $g \sim 2.0$ for Mn^{2+} ions, we have calculated the values of total quantum number (J) per formula unit for the samples as listed in table 1.

Table 2. EDAX data of $Zn_{0.95}Mn_{0.02}Sb_yO$ samples.

Sample	Zn (at.%)	Mn (at.%)	Sb (at.%)	O (at.%)
$y = 0.0$	52.10	1.68	—	46.22
$y = 0.01$	61.27	1.75	1.19	35.79
$y = 0.03$	61.68	1.57	2.37	34.38

We have also calculated the value of effective exchange interaction constant (J_{ex}) for a proper understanding of the nature of AFM interaction in these samples using the relation

$$J_{\text{ex}} = 3\theta(x)k_B/2 \times J(J+1)Z_{\text{NN}} \tag{5}$$

where x ($x \sim 0.02$) is the atomic fraction of magnetic ions and Z_{NN} is the number of nearest neighbors ($Z_{\text{NN}} = 12$). From the calculation of J_{ex}, using the values of the required parameters from table 1, the values of $2J_{\text{ex}}/k_B$ are found to be −16.49 and −8.13 K for $Zn_{0.98}Mn_{0.02}O$ and $Zn_{0.95}Mn_{0.02}Sb_{0.03}O$ samples, respectively. The higher values of $2J_{\text{ex}}/k_B$ with negative sign clearly indicate the presence of strong AFM interactions in the samples. Moreover, the magnitudes of $2J_{\text{ex}}/k_B$ values with negative sign are found to decrease with co-doping of Sb, indicating a decrease in AFM interaction in the sample with co-doping of Sb.

Microstructural and chemical analyses of the samples were done using FESEM–EDAX. From the FESEM micrographs, we found that as we go from pure the ZnMnO sample to the Sb co-doped ZnMnO sample there is a two fold decrease in the grain size (see figure 6). These results are in agreement with the XRD results (see figure 2). The EDAX results for all the samples are listed in table 2. From the EDAX data it is found that the sample with a larger grain size ($y = 0$) has a higher oxygen content, i.e. fewer oxygen vacancies, than samples with a smaller grain size ($y = 0.01$ and 0.03). In the present case there may also be some contribution of Zn vacancies in introducing ferromagnetism in the sample as reported by Iusan *et al* [28] on the basis of theoretical calculation. A representative EDAX pattern of the $Zn_{0.95}Mn_{0.02}Sb_{0.03}O$ sample, showing the presence of Sb, Mn, Zn and O, is shown in figure 7. We do not observe any clustering of Mn or Co in the samples through FESEM–EDAX results or from XRD results within the detection limits of both techniques.

Thus from the magnetic measurements we see that Sb co-doping helps in stabilizing RTFM in ZnMnO. Although the exact mechanism for the observed RTFM is not clear, the experimental results of the present investigation clearly suggest that not only the presence of carriers but also the defects (associated with strain, i.e. oxygen vacancies and defects at zinc sites) play an important role in introducing

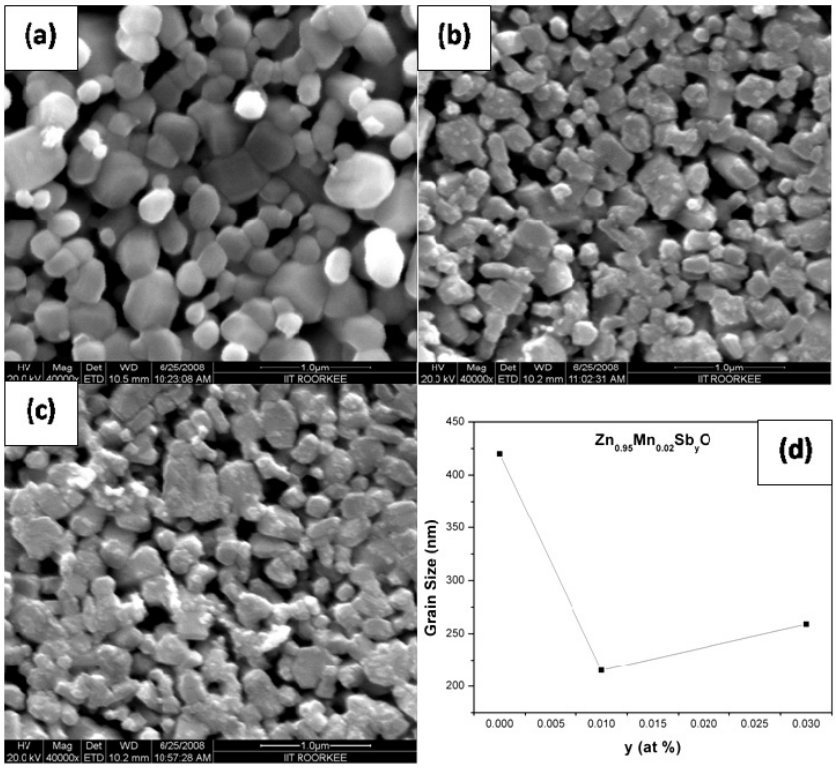

Figure 6. FESEM micrographs of $Zn_{0.98}Mn_{0.02}Sb_yO$: (a) $y = 0$, (b) $y = 0.01$ and (c) $y = 0.03$. (d) The variation of average grain size with Sb co-doping concentration.

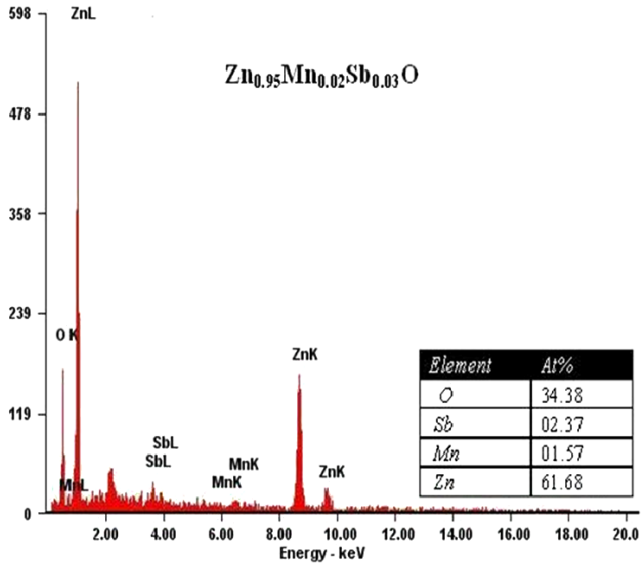

Figure 7. Typical EDAX pattern of $Zn_{0.98}Mn_{0.02}Sb_{0.03}O$ sample.

FM in the samples. Strain induced FM is also reported in ZnCoO thin films [29]. Oxygen vacancy induced RTFM has been reported by several groups [30–32]. In our samples, we were not able to measure the carrier concentration due to their high resistance. Thus right now we are not sure that the observed RTFM in Sb co-doped ZnMnO samples is due to additional carriers introduced by Sb co-doping. However, based on the experimental results, we conclude that the observed RTFM in Sb co-doped ZnMnO samples is due to defects induced by strain. Recently, RTFM in Sb co-doped ZnMnO thin films was reported by Ji *et al* [20]. They found ferromagnetism in $Zn_{0.985}(Mn_{0.01}Sb_{0.005})O$ with $M_S \sim 0.92\ \mu_B/Mn^{2+}$ and this value increases further to $1.76\ \mu_B/Mn^{2+}$ after annealing the samples in an oxygen rich atmosphere. They explained the observed FM by the bound magnetic polaron (BMP) [33] model, in which localized p-type defects mediate the ferromagnetic ordering. In our case the value of M_S ($\sim 0.082 \times 10^{-3}\ \mu_B$/Mn) is small in comparison to the one reported by Ji *et al*. The difference in magnetic moment values is possibly due to the sensitivity of the DMS materials to the synthesis conditions and synthesis techniques. Moreover in our case the ferromagnetism is due to oxygen vacancies which give rise to n-type behavior [34]. Further characterizations to understand the origin of ferromagnetism are under progress.

4. Conclusions

In summary, we observed RTFM in Sb co-doped ZnMnO samples synthesized by a solid state reaction route. Based on the experimental results it has been concluded that the defects induced by strain play an important role in stabilizing RTFM in Sb co-doped ZnMnO samples.

Acknowledgment

One of the authors (V K Sharma) is grateful to CSIR, Government of India, for a research fellowship.

References

[1] Dietl T, Ohno H, Matsukura F, Cibert J and Ferrand D 2000 *Science* **287** 1019
[2] Cheng X M and Chien C L 2003 *J. Appl. Phys.* **93** 7876
[3] Kolesnik S and Dabrowski B 2004 *J. Appl. Phys.* **96** 5379
[4] Jung S W, An S J, Yi G C, Jung C U, Lee S I and Cho S 2002 *Appl. Phys. Lett.* **80** 4561
[5] Pradhan A K, Zhang K, Mohanty S, Dadson J B, Hunter D, Zhang J, Sellmeyer D J, Roy U N, Chui Y, Burger A, Matthews S, Joseph B, Sekhar B R and Roul B K 2005 *Appl. Phys. Lett.* **86** 152511
[6] Sluiter M H F, Kawazoe Y, Sharma P, Inoue I, Raju A R, Rout C and Waghmare U V 2005 *Phys. Rev. Lett.* **94** 187204
[7] Sandratskii L M and Bruno P 2006 *Phys. Rev.* B **73** 045203
[8] Janisch R, Gopal P and Spaldin N A 2005 *J. Phys.: Condens. Matter* **17** R657
[9] Fukumura T, Jin Z, Kawasaki M, Shono T, Hasegawa T, Koshihara S and Koinuma H 2001 *Appl. Phys. Lett.* **78** 958
[10] Lin H T, Chin T S, Shih J C, Lin S H, Hong T M, Huang R T, Chen F R and Kai J J 2004 *Appl. Phys. Lett.* **85** 621
[11] Manivannan A, Glaspell G, Dutta P and Seehra M S 2005 *J. Appl. Phys.* **97** 10D325
[12] Liu X C, Shi E W, Chen Z A, Huang H W, Xiao B and Song X L 2006 *Appl. Phys. Lett.* **88** 252503
[13] Fukumura T, Jin Z, Ohtomo A, Koinuma H and Kawasaki M 1999 *Appl. Phys. Lett.* **75** 3366
[14] Jin Z, Fukumura T, Kawasaki M, Ando K, Saito H, Sekiguchi T, Yoo Y Z, Murakami M, Matsumoto Y, Hasegawa T and Koinuma H 2001 *Appl. Phys. Lett.* **78** 3824
[15] Zhang T, Song L X, Chen Z Z, Shi E W, Chao L X and Zhang H W 2006 *Appl. Phys. Lett.* **89** 172502
[16] Liu X J, Song C, Zeng F and Pan F 2007 *J. Phys.: Condens. Matter* **19** 296208
[17] Hu X H, Blythe H J, Ziese M, Behan A J, Neal J R, Mokhtari A, Ibrahim R M, Fox A M and Gehring G A 2006 *New J. Phys.* **8** 135
[18] Jayakumar O D, Gopalakrishnan I K and Kulshreshtha S K 2005 *J. Mater. Chem.* **15** 3514
[19] Chakraborti D, Ramachandran S, Trichy G, Narayan J and Prater J T 2007 *J. Appl. Phys.* **101** 053918
[20] Ji G H, Gu Z B, Lu M H, Wu D, Zhang S T, Zhu Y Y, Zhu S N and Chen Y F 2008 *J. Phys.: Condens. Matter* **20** 425207
[21] Akoi T, Shimizu Y, Miyake A, Nakamura A, Nakanishi Y and Hatanaka Y 2002 *Phys. Status Solidi* b **229** 911
[22] Xiu X F, Yang Z, Mandalapu L J, Zhao D T, Liu J L and Beyermann W P 2005 *Appl. Phys. Lett.* **87** 152101
[23] Williamson G K and Hall W H 1953 *Acta Metall.* **1** 22
[24] Kameli P, Salamati H and Aezami A 2006 *J. Appl. Phys.* **100** 053914
[25] Reimers J N, Greedman J E and Subramanian M A 1989 *J. Solid State Chem.* **79** 263
[26] Han S J, Jang T H, Kim Y B, Park B G, Park J H and Jeong Y H 2003 *Appl. Phys. Lett.* **83** 920
[27] Norton D P, Pearton S J, Hebard A F, Theodoropoulou N, Boatner L A and Wilson R G 2003 *Appl. Phys. Lett.* **82** 239
[28] Iusan D, Sanyal B and Eriksson O 2006 *Phys. Rev.* B **74** 235208
[29] Liu X J, Song C, Zeng F, Pan F, He B and Yan W S 2008 *J. Appl. Phys.* **103** 093911
[30] Sharma V K and Varma G D 2007 *J. Appl. Phys.* **102** 056105
[31] Hsu H S, Huang J C A, Huang Y H, Liao Y F, Lin M Z, Lee C H, Lee J F, Chen S F, Lai L Y and Liu C P 2006 *Appl. Phys. Lett.* **88** 242507
[32] Ramachandran S, Narayan J and Prater J T 2006 *Appl. Phys. Lett.* **88** 242503
[33] Coey J M D, Venkatesan M and Fitzgerald C B 2005 *Nat. Mater.* **4** 173
[34] Manivannan A, Dutta P, Glaspell G and Seehra M S 2006 *J. Appl. Phys.* **99** 08M110